ESCA, Solid-State NMR, and X-ray Diffraction Monitor the Hydrogen Bonding in a Complex of 1,8-Bis(dimethylamino)naphthalene with 1,2-Dichloromaleic Acid

ARTICLE *in* THE JOURNAL OF PHYSICAL CHEMISTRY · OCTOBER 1995

Impact Factor: 2.78 · DOI: 10.1021/j100040a014

5 AUTHORS, INCLUDING:

Krzysztof Wozniak
University of Warsaw
313 PUBLICATIONS **3,404** CITATIONS
SEE PROFILE

Jacek Klinowski
University of Cambridge
537 PUBLICATIONS **16,453** CITATIONS
SEE PROFILE

ESCA, Solid-State NMR, and X-ray Diffraction Monitor the Hydrogen Bonding in a Complex of 1,8-Bis(dimethylamino)naphthalene with 1,2-Dichloromaleic Acid

Krzysztof Wozniak,[†,‡] Heyong He,[‡] Jacek Klinowski,*[,‡] William Jones,[‡] and Tery L. Barr[§]

Department of Chemistry, University of Warsaw, 02-093 Warszawa, ul. Pasteura 1, Poland, Department of Chemistry, University of Cambridge, Lensfield Road, Cambridge CB2 1EW, U.K., and Department of Materials, Laboratory for Surface Studies, University of Wisconsin—Milwaukee, Milwaukee, Wisconsin 53201

Received: June 13, 1995; In Final Form: August 1, 1995[⊗]

The complex of 1,8-bis(dimethylamino)naphthalene (DMAN) with 1,2-dichloromaleic acid ($ClMH_2$) has been examined by electron spectroscopy (ESCA), X-ray diffraction at 120 and 293 K, and ^{13}C and ^{1}H MAS NMR at 123 and 293 K. The complex contains two strong, asymmetric, ionic hydrogen bonds, $[N-H\cdots N]^+$ and $[O-H\cdots O]^-$. The asymmetry results from asymmetric intermolecular interactions of the oxygen atoms of the carboxylic groups. Well-resolved ^{13}C MAS NMR spectra of a DMAN salt show separate signals from protonated "almost symmetrical" carbons. The difference between the binding energies of core (and valence) electrons of the donor and acceptor atoms is a good measure of the strength of hydrogen bonds. The influence of hydrogen bonding on the binding energies of core electrons of the atoms of the $ClMH^-$ anion decreases with the increased distance from the $[O-H\cdots O]^-$ hydrogen bond site.

Introduction

Electron spectroscopy for chemical analysis (ESCA) is known to be a powerful method of surface analysis.[1−3] A sample is irradiated with monoenergetic soft X-rays (Al Kα or Mg Kα), and the energies of emitted electrons are monitored. The photons penetrate the outermost layer of the solid to the depth of ca. 1−10 μm and interact with atoms in that surface region via the photoelectric effect causing electrons to be emitted. The kinetic energy of the emitted electrons is

$$KE = h\nu - BE - \Phi_s$$

where $h\nu$ is the energy of the photon, BE is the binding energy of the atomic orbital from which the electron originates, and Φ_s is the spectrometer work function. Since each type of atom can give rise to a variety of different ions, there is a corresponding variety of kinetic energies of emitted electrons. Although ionization occurs up to a depth of a few micrometers, only electrons emitted within tens of angstroms below the surface can leave the sample and be detected. Other electrons lose energy while passing through the solid. Thus ESCA is well attuned to the observation of surface phenomena.

The aim of this work is to examine the influence of strong hydrogen bonds on the binding energies of the core electrons of atoms involved in hydrogen bonding and atoms which are remote from the hydrogen bond sites. We have selected a complex of the aromatic diamine 1,8-bis(dimethylamino)-naphthalene (DMAN) with 1,2-dichloromaleic acid ($ClMH_2$) (Figure 1). DMAN belongs to the class of compounds with extremely high basicity constants and proton affinities, known as proton sponges. With mineral or organic acids, proton sponges form very stable ionic complexes containing intramolecular $[N\cdots H\cdots N]^+$ hydrogen bonds. Proton sponges have attracted considerable attention, particularly since the reviews by Staab[4] and Alder[5] appeared, and more than 70 X-ray structures have been published. Intramolecularly hydrogen-bonded proton sponges have been the subject of more than 100 papers. The DMAN molecule itself has been studied by X-ray diffraction,[6,7] solid-state NMR,[7−9] NQR[7,10,11] at 293 K and low temperatures and ab-initio computational methods.[12]

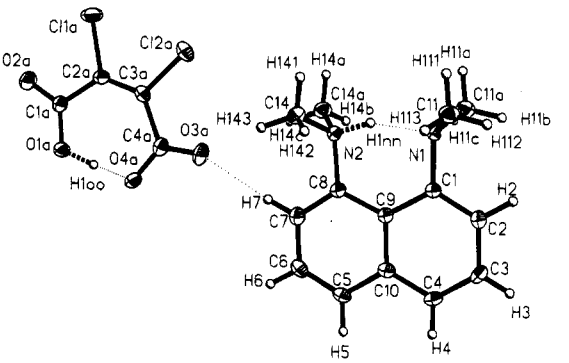

Figure 1. Numbering scheme and atomic displacement parameters for the $DMANH^+$ and $ClMH^-$ ions at 120 K. The ellipsoids are drawn at the 50% probability level.

The Cambridge Structural Database[13] contains nearly 50 structures involving the hydrogen maleate anion and its derivatives, including the complexes of maleic acid with 1,8-diaminonaphthalene[14] and 1,8-bis(dimethylamino)naphthalene.[15] Ab-initio computational methods were also used to study this model moiety.[16,17] One can expect the $[N-H\cdots N]^+$ hydrogen bond in the $DMANH^+$ cation and the $[O-H\cdots O]^-$ hydrogen bond in the $ClMH^-$ anion to influence significantly the ESCA spectra of the $DMANH^+ClMH^-$ complex.

Experimental Section

Synthesis. $DMANH^+ClMH^-$ was prepared by mixing maleic acid with DMAN in acetonitrile. The product was then recrystallized from methanol.

X-ray Diffraction. Crystals of DMAN suitable for X-ray work were grown from heptane by slow evaporation. X-ray measurements were made on a Rigaku AFC7R diffractometer using monochromated Mo Kα radiation in the $\omega-2\theta$ scan mode. Three standard reflections were monitored for every 100 reflections collected, and none showed a significant decrease

[†] University of Warsaw.
[‡] University of Cambridge.
[§] University of Wisconsin—Milwaukee.
[⊗] Abstract published in *Advance ACS Abstracts,* September 15, 1995.

0022-3654/95/2099-14667$09.00/0

TABLE 1: Crystal Data and Structure Refinement Details at 293 and 120 K

identification code	DMANH$^+$ClMH$^-$	
empirical formula	$C_{18}H_{20}Cl_2N_2O_4$	
formula weight	399.27	
color	colorless	
temperature [K]	293(2)	120(2) K
wavelength [Å]	0.71073	
crystal system	orthorhombic	
space group	*Pnma*	
unit cell dimensions		
a [Å]	18.211(1)	18.086(1)
b [Å]	7.134(1)	6.983(1)
c [Å]	14.405(1)	14.363(1)
volume [Å^3]	1871.5(3)	1814.0(3)
Z	4	
density (calcd) [Mg/m^3]	1.417	1.462
absorption coefficient [mm^{-1}]	0.385	
F (000)	832	
crystal size [mm]	0.25 × 0.20 × 0.30	0.20 × 0.35 × 0.30
θ range for data collection [deg]	2.4−25	2.7−35
index ranges	$-2 \le h \le 25$	$0 \le h \le 21$
	$-2 \le k \le 10$	$-11 \le k \le 8$
	$-2 \le l \le 20$	$-13 \le l \le 17$
reflections collected	3109	7074
independent reflections	1797	1948
R (int)	0.0287	0.020
refinement method	full-matrix least-squares on F^2	
data/restraints/parameters	1788/0/200	1942/0/200
goodness-of-fit	1.034	1.045
final *R* indices [$I > 2\sigma(I)$]		
*R*1,*wR*2	0.0444, 0.1035	0.0331, 0.0853
R indices (all data)		
*R*1, $\omega R2$	0.0824, 0.1293	0.0466, 0.0971
largest diff. peak/hole [e Å^{-3}]	0.193/−0.217	0.298/−0.217

in standard intensity over the data collection time. The data were corrected for the Lorentz and polarization effects,[18] and the structure was solved by direct methods[19] and refined using SHELXL-93.[20] The refinement was based on F^2 for all reflections except those with very negative F^2. Weighted *R* factors ωR and all goodnesses-of-fit *S* values are based on F^2. Conventional *R* factors are based on *F* with *F* set to zero for negative F^2. The criterion $F_o^2 > 2\sigma(F_o^2)$ was used only for calculating *R* factors and is not relevant to the choice of reflections for the refinement. *R* factors based on F^2 are about twice as large as those based on *F*, and *R* factors based on all data are even larger. Scattering factors and absorption coefficients were taken from Tables 6.1.1.4 and 4.2.4.2 in ref 21. Experimental details concerning the collection and refinement of data are listed in Table 1.

Solid-State NMR. ^{1}H magic-angle-spinning (MAS) NMR spectra and ^{13}C spectra with MAS and ^{1}H−^{13}C cross-polarization (CP/MAS) were recorded at 293 and 123 K at 399.9 and 100.6 MHz, respectively, using a Chemagnetics CMX-400 multinuclear spectrometer. Zirconia rotors were spun in nitrogen gas at different rates in order to identify sidebands and resonance overlaps. ^{1}H MAS NMR spectra were measured with spinning at 9−12 kHz using 2 μs (30°) pulses and 3 s recycle delays. Single contact ^{1}H−^{13}C CP/MAS experiments were performed with 4 ms contact times and short-contact-time experiments with 50 μs contact times. The ^{1}H $\pi/2$ pulses were typically 2.5 μs, the recycle delay 3 s, and the MAS rate 5−9 kHz. Dipolar-dephased ^{1}H−^{13}C spectra were recorded with a 50 μs delay prior to acquisition, 4 ms contact time, and 3 s recycle delays. Conventional MAS spectra contain resonances from all carbons, while dipolar-dephased spectra identify resonances from quaternary carbons and short-contact-time CP spectra reveal the protonated carbons.

ESCA. ESCA spectra were recorded on a Hewlett-Packard 5950A spectrometer equipped with a high-resolution X-ray monochromator. A conventional Al Kα anode was used as a source of radiation. The background pressure during analysis was ca. 1×10^{-9} Torr. The material under study is an insulator and produces distinctive charging shifts[22] because the sample does not have sufficient delocalized conductive electrons available to neutralize the charged centers formed by clustering of the positive holes created as a result of photoelectron ejection. Photoelectric processes lead to the formation of ions in the ground state, which builds a positive outer potential near the surface producing an additional positive shift in binding energies of the outgoing electrons. The charging shifts were removed and the binding scale established using a combination of electron flood guns and fixing the C(1s) binding energy of hydrocarbon carbons at 284.6 eV. This well-established procedure has been successfully applied in a number of studies.[2,23] A broad survey scan in the 0−1000 eV scan range was used to identify the elements present. Detailed scans (20 eV wide) recorded for precise peak location were used for peak deconvolution. The C(1s) line used for charge referencing was measured at the beginning, in the middle, and at the end of data collection, and its position was constant with time.

Results and Discussion

X-ray Analysis. The DMANH$^+$ClMH$^-$ crystallizes in the orthorhombic *Pnma* space group with four molecules in the unit cell (Table 1). The unit cell parameters are $a = 18.211(1)$ Å, $b = 7.134(1)$ Å, and $c = 14.405(1)$ Å at 293 K and 18.086(1) Å, 6.983(1) Å, and 14.363(1) Å at 120 K. Decreased temperature thus causes a small decrease in unit cell parameters (0.125 Å, 0.151 Å, and 0.042 Å for *a*, *b* and *c*, respectively). All positions of hydrogen atoms were obtained from difference electron density maps. Estimated standard deviations (esd's) were found using the full covariance matrix and were taken into account individually in the calculation of esd's for distances, angles, and torsion angles. The labeling of atoms in the asymmetric unit and the atomic displacement parameters are given in Figure 1, the positional parameters in Table 2, and the

TABLE 2: Atomic Coordinates (× 10^4) and Equivalent Isotropic Displacement Parameters (Å² × 10^3) for Non-Hydrogen Atoms and Isotropic Displacement Parameters (Å² × 10^3) for Hydrogens in DMANH⁺ClMH⁻. *U*(eq) Is Defined as One-Third of the Trace of the Orthogonalized *Uij* Tensor. Hydrogen Coordinates (× 10^3)

	293 K				120 K			
atom	*x*	*y*	*z*	*U*(eq)/*U*(iso)	*x*	*y*	*z*	*U*(eq)/*U*(iso)
N(1)	2669(1)	2500	8534(2)	44(1)	2674(1)	2500	8541(1)	17(1)
N(2)	1535(2)	2500	9673(2)	44(1)	1525(1)	2500	9674(1)	17(1)
C(1)	2162(2)	2500	7753(2)	41(1)	2167(1)	2500	7755(1)	17(1)
C(2)	2415(2)	2500	6862(3)	58(1)	2427(1)	2500	6859(2)	23(1)
C(3)	1935(2)	2500	6105(3)	62(1)	1947(1)	2500	6090(2)	25(1)
C(4)	1201(2)	2500	6253(3)	57(1)	1200(1)	2500	6235(2)	22(1)
C(5)	143(2)	2500	7310(3)	58(1)	129(1)	2500	7285(2)	23(1)
C(6)	−134(2)	2500	8172(3)	67(1)	−160(1)	2500	8161(2)	27(1)
C(7)	324(2)	2500	8948(3)	58(1)	304(1)	2500	8942(2)	24(1)
C(8)	1065(2)	2500	8834(2)	42(1)	1050(1)	2500	8834(2)	18(1)
C(9)	1394(2)	2500	7942(2)	39(1)	1391(1)	2500	7933(2)	16(1)
C(10)	909(2)	2500	7158(2)	45(1)	905(1)	2500	7146(2)	18(1)
C(11)	3124(2)	794(5)	8556(2)	62(1)	3132(1)	753(2)	8565(1)	24(1)
C(14)	1439(2)	773(4)	10246(2)	59(1)	1420(1)	743(2)	10255(1)	24(1)
Cl(1a)	−399(1)	2500	14470(1)	108(1)	−407(1)	2500	14492(1)	43(1)
Cl(2a)	447(1)	2500	12679(1)	79(1)	447(1)	2500	12694(1)	29(1)
O(1a)	−2139(1)	2500	12938(2)	68(1)	−2169(1)	2500	12935(1)	27(1)
O(2a)	−1915(2)	2500	14417(2)	84(1)	−1942(1)	2500	14438(1)	32(1)
O(3a)	−341(2)	2500	11018(2)	93(1)	−334(1)	2500	11019(1)	35(1)
O(4a)	−1476(2)	2500	11518(2)	69(1)	−1488(1)	2500	11510(1)	26(1)
C(1a)	−1708(2)	2500	13628(3)	55(1)	−1730(1)	2500	13636(2)	22(1)
C(2a)	−878(2)	2500	13442(2)	52(1)	−894(1)	2500	13452(2)	21(1)
C(3a)	−501(2)	2500	12639(3)	50(1)	−508(1)	2500	12650(2)	20(1)
C(4a)	−781(2)	2500	11638(3)	57(1)	−788(1)	2500	11643(2)	23(1)
H(1nn)	200(2)	250	939(3)	69(12)	204(2)	250	940(2)	30(7)
H(1oo)	−189(3)	250	1229(3)	103(16)	−188(2)	250	1227(3)	98(15)
H(141)	181(2)	84(4)	1074(2)	79(9)	180(1)	77(3)	1073(1)	31(5)
H(142)	152(1)	−35(4)	984(2)	77(9)	150(1)	−39(3)	988(1)	32(5)
H(143)	93(1)	71(4)	1050(2)	69(8)	90(1)	74(3)	1051(1)	30(5)
H(111)	344(1)	85(4)	911(2)	62(7)	344(1)	80(3)	913(1)	23(4)
H(112)	344(1)	72(4)	800(2)	67(8)	345(1)	64(3)	803(1)	35(5)
H(113)	280(1)	−31(4)	853(2)	63(8)	282(1)	−37(3)	857(1)	26(5)
H(2)	294(2)	250	673(2)	64(11)	297(2)	250	675(2)	33(7)
H(3)	214(2)	250	550(3)	61(11)	213(1)	250	551(2)	25(7)
H(4)	88(2)	250	580(2)	52(10)	87(1)	250	575(2)	23(6)
H(5)	−18(2)	250	681(3)	65(11)	−19(2)	250	675(2)	32(7)
H(6)	−67(2)	250	829(3)	70(11)	−68(2)	250	828(2)	31(7)
H(7)	10(2)	250	952(3)	67(12)	10(2)	250	954(2)	37(8)

selected bond lengths and angles in Table 3. The packing of the DMANH⁺ClMH⁻ molecules in the crystal lattice is shown in Figure 2. All anisotropic thermal parameters as well as the observed and calculated structure factors have been deposited as Supporting Information.

The asymmetric unit of DMANH⁺ClMH⁻ consists of the coplanar DMANH⁺ cation and the ClMH⁻ anion (Figure 1). The crystal structure is built up from layers of molecules. As a result of strong electrostatic interactions, each cation in every layer (Figure 3) is surrounded by four anions and vice versa. Alternating layers of cations and anions are found at Y = 0.25 and Y = 0.75 (Figure 2b). The neighboring columns of moieties are shifted relative to each other by 0.5 of a unit along the *Y* axis. As a result, every DMANH⁺ cation is surrounded by six negatively charged ClMH⁻ moieties and vice versa. As a consequence of the very strong electrostatic interactions between the ions in the crystal, some relatively short intermolecular contacts are very likely to occur. The shortest of them can be considered as a potential weak C−H···O hydrogen bond donated by the cation. The geometry of these weak hydrogen bonds is given in Table 4. Analysis of the shortest nonbonded distances shows that each anion interacts along a diagonal with two cations via weak C−H···O hydrogen bonds forming characteristic zig−zag patterns. The neighboring zig−zags complement each other (Figure 3). This is a good illustration that weak C−H···O interactions "fine-tune" the general structural pattern formed by the stronger electrostatic interactions.

The DMANH⁺ cation is planar and located at the *m* symmetry plane. As a result, only two out of the four methyl groups of DMANH⁺ are independent. The [N−H···N]⁺ hydrogen bond is relatively long (N1···N2 = 2.638(4) Å) compared to the shortest hydrogen bridges in the DMAN salts of ca. 2.55 Å. It is asymmetric with the N2−H1nn distance of 0.95(4) Å and the N1···H1nn contact of 1.72(4) Å. The geometries of the [N−H···N]⁺ hydrogen bond and of the cation are close to those reported for other DMAN salts.[24−35]

The asymmetric [N−H···N]⁺ hydrogen bond is primarily reflected in the valence angles. The most significant differences between similar bond angles in the two halves of the DMAN moiety are for the N2C8C9 and N1C1C9 (119.7(3)° and 118.4(3)°), C7C8C9 and C9C1C2 (122.0(3)° and 120.7(3)°), C7C8N2 and C2C1N1 (118.4(3)° and 120.9(3)°), C6C7C8 and C1C2C3 (119.8(4)° and 121.5(3)°), and C5C6C7 and C4C3C2 (121.1(3)° and 119.7(4)°) bond angles. The asymmetry is caused by the transmission of the electronic effects of the asymmetric [N···H···N]⁺ hydrogen bonding through endocyclic angles at C8 and C1. There is only one significant difference between similar bond lengths in the two halves of the cation. The N2C8 and N1C1 bond lengths are 1.481(4) and 1.454(4) Å, respectively. The structure of the cation at 120 K shows similar features because of a different degree of attenuation of substituent effects of protonated and nonprotonated−NMe_2 groups in the two halves of the cation. The C1N1C11 and C8N2C14 bond angles are slightly larger than the typical values for pure sp^3 hybridization. Also the C14−N2 bond lengths are

TABLE 3: Selected Geometrical Parameters: Bond Lengths [Å] and Angles [deg] for DMANH$^+$ClMH$^-$

parameter	293 K	120 K
	Bond Lengths	
N(1)−C(1)	1.454(4)	1.454(3)
N(1)−C(11)[a]	1.473(3)	1.475(2)
N(1)−C(11)	1.473(3)	1.475(2)
N(2)−C(8)	1.481(4)	1.481(3)
N(2)−C(14)	1.493(3)	1.496(2)
N(2)−H(1nn)	0.95(3)	1.02(3)
C(1)−C(2)	1.363(5)	1.371(3)
C(1)−C(9)	1.425(4)	1.425(3)
C(2)−C(3)	1.398(5)	1.405(3)
C(3)−C(4)	1.353(5)	1.366(3)
C(4)−C(10)	1.408(5)	1.413(3)
C(5)−C(6)	1.340(6)	1.362(3)
C(5)−C(10)	1.413(5)	1.419(3)
C(6)−C(7)	1.395(5)	1.401(3)
C(7)−C(8)	1.358(4)	1.358(3)
C(8)−C(9)	1.418(4)	1.433(3)
C(9)−C(10)	1.434(4)	1.433(3)
Cl(1a)−C(2a)	1.718(3)	1.734(2)
Cl(2a)−C(3a)	1.726(3)	1.729(2)
O(1a)−C(1a)	1.266(4)	1.283(3)
O(1a)−H(1oo)	1.04(5)	1.09(4)
O(2a)−C(1a)	1.197(4)	1.213(3)
O(3a)−C(4a)	1.201(4)	1.214(3)
O(4a)−C(4a)	1.276(4)	1.282(3)
O(4a)−H(1oo)	1.34(5)	1.30(4)
C(1a)−C(2a)	1.536(5)	1.536(3)
C(2a)−C(3a)	1.346(5)	1.347(3)
C(3a)−C(4a)	1.530(5)	1.532(3)
	Bond Angles	
C(2a)−C(3a)−Cl(2a)	118.8(3)	119.1(2)
C(4a)−C(3a)−Cl(2a)	111.4(3)	111.3(2)
O(3a)−C(4a)−O(4a)	124.2(4)	123.9(2)
O(3a)−C(4a)−C(3a)	118.6(4)	118.3(2)
O(4a)−C(4a)−C(3a)	117.3(3)	117.8(2)
C(1)−N(1)−C(11)	111.9(2)	111.9(1)
C(11)[a]−N(1)−C(11)	111.5(3)	111.6(2)
C(8)−N(2)−C(14)	112.6(2)	112.4(1)
C(14)−N(2)−C(14)[a]	111.2(3)	110.2(2)
C(8)−N(2)−H(1nn)	99(2)	102.5(14)
C(14)−N(2)−H(1nn)	110(1)	109.5(7)
C(14)[a]−N(2)−H(1nn)	110(1)	109.5(7)
C(2)−C(1)−C(9)	120.7(3)	120.4(2)
C(2)−C(1)−N(1)	120.9(3)	120.8(2)
C(9)−C(1)−N(1)	118.4(3)	118.8(2)
C(1)−C(2)−C(3)	121.5(3)	121.7(2)
C(4)−C(3)−C(2)	119.7(4)	119.4(2)
C(3)−C(4)−C(10)	121.2(3)	121.0(2)
C(6)−C(5)−C(10)	121.0(3)	120.6(2)
C(5)−C(6)−C(7)	121.1(3)	120.7(2)
C(8)−C(7)−C(6)	119.8(4)	120.2(2)
C(7)−C(8)−C(9)	122.0(3)	122.1(2)
C(7)−C(8)−N(2)	118.4(3)	118.8(2)
C(9)−C(8)−N(2)	119.7(3)	119.1(2)
C(8)−C(9)−C(1)	126.0(3)	125.8(2)
C(8)−C(9)−C(10)	116.9(3)	116.7(2)
C(1)−C(9)−C(10)	117.1(3)	117.5(2)
C(4)−C(10)−C(5)	121.1(3)	120.3(2)
C(4)−C(10)−C(9)	119.7(3)	120.0(2)
C(5)−C(10)−C(9)	119.2(3)	119.7(2)
C(1a)−O(1a)−H(1oo)	116(3)	113(2)
C(4a)−O(4a)−H(1oo)	116(3)	114(2)
O(2a)−C(1a)−O(1a)	123.4(4)	123.4(2)
O(2a)−C(1a)−C(2a)	118.4(3)	118.3(2)
O(1a)−C(1a)−C(2a)	118.2(3)	118.3(2)
C(3a)−C(2a)−C(1a)	130.7(3)	131.1(2)
C(3a)−C(2a)−Cl(1a)	118.8(3)	118.3(2)
C(1a)−C(2a)−Cl(1a)	110.5(3)	110.6(2)
C(2a)−C(3a)−C(4a)	129.8(3)	129.6(2)

[a] x, $^1/_2 - y$, z.

elongated by 0.020 Å compared to the N1CMe bond. This is consistent with the localization of the proton at the N2 nitrogen atom.

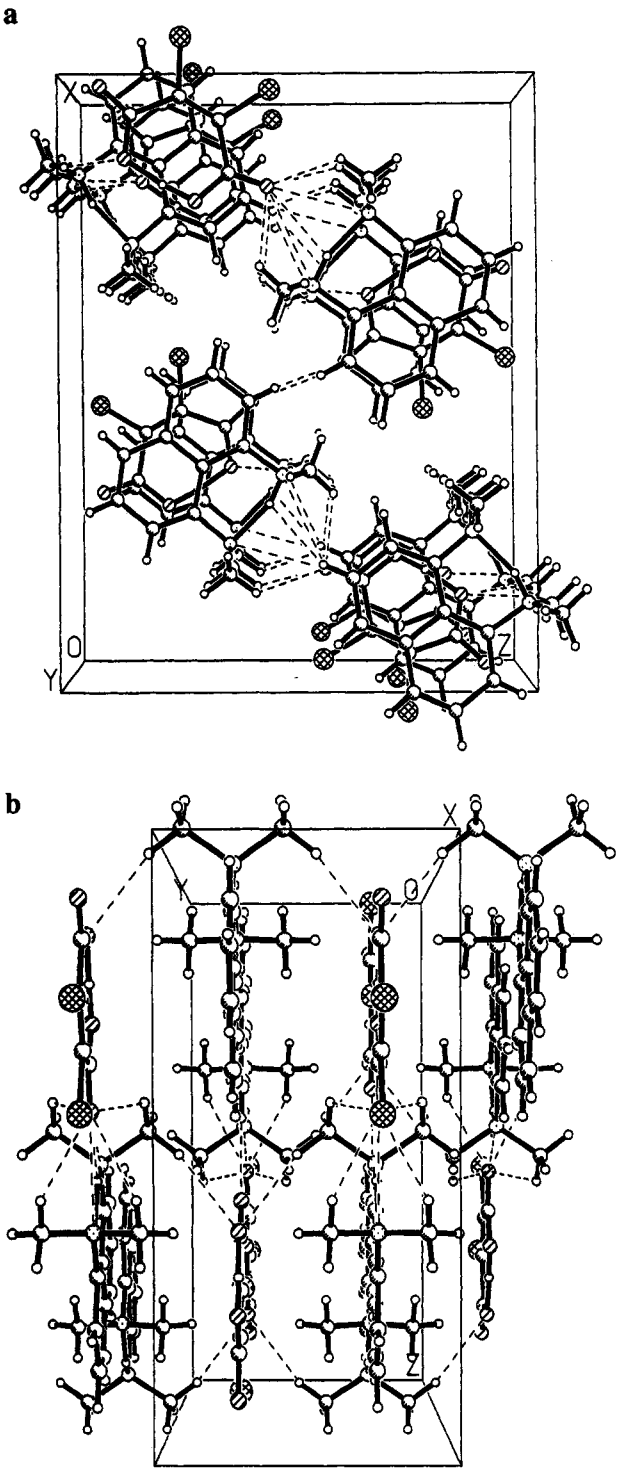

Figure 2. Packing of the DMANH$^+$ClMH$^-$ molecules in the crystal lattice: (a) *XY* projection and (b) *YZ* projection.

The geometry of the cation closely resembles the ab-initio calculated geometry of the symmetric DMANH$^+$ cation[12] with deviations of 0.020 and 0.018 Å for C6C5 and C6C7 bond lengths, respectively. All other differences are less than 0.010 Å. In the case of the bond angles the largest differences are between C8C9C1, C9C8N2, and C8N2C14 angles (1.7°, 2.3°, and 2.2°, respectively). These values reflect the expected differences in structural parameters when the asymmetric [N−H···N]$^+$ hydrogen bond in proton sponges is compared with the symmetric [N···H···N]$^+$ bond. The agreement of the 120 K structural parameters with the calculated ones is slightly better.

In general, the structure of DMANH$^+$ClMH$^-$ at 120 K is very similar to the room temperature structure with the largest differences being 0.022(7), 0.017(5) and 0.016(5) Å for the

TABLE 4: Geometry of Hydrogen Bonds in DMANH$^+$ClMH$^-$

temp [K]	D−H [Å]	H···A [Å] symmetry	D···A [Å]	DHA [deg]
	N2−H1nn	H1nn···N1	N2···N1	N2−H1nn−N1
293	0.95(4)	1.72(4)	2.638(4)	161(2)
120	1.02(3)	1.68(3)	2.640(4)	156(2)
	O1a−H1oo	H1oo···O4a	O1aa···O4a	O1a−H1oo−O4a
293	1.04(5)	1.34(5)	2.376(4)	172(4)
120	1.09(4)	1.30(5)	2.389(2)	177(4)
	C11−H111	H111···O2a $0.5+X, Y, 2.5-Z$	C11···O2a	C11−H111−O2a
293	0.98(4)	2.51(4)	3.164(4)	124(3)
120	0.98(3)	2.47(3)	3.119(3)	124(2)
	C14−H141	H141···O2a $0.5+X, Y, 2.5-Z$	C14···O2a	C14−H141−O2a
293	0.98(4)	2.62(4)	3.277(4)	125(3)
120	0.96(3)	2.59(3)	3.237(3)	124(2)
	N2−H1nn	H1nn···O2a $0.5+X, Y, 2.5-Z$	N2···O2a	N2−H1nn−O2a
293	0.95(4)	2.62(4)	3.113(4)	113(3)
120	1.02(3)	2.48(3)	3.053(3)	115(2)
	C7−H7	H7···O3a	C7···O3a	C7−H7−O3a
293	0.92(4)	2.31(4)	3.219(3)	175(3)
120	0.93(3)	2.27(3)	3.199(3)	176(2)
	C14−H142	H142···O4a $-X, -Y, 2-Z$	C14···O4a	C14−H141−O4a
293	0.97(4)	2.48(4)	3.451(3)	159(3)
120	1.00(3)	2.49(3)	3.401(2)	161(2)

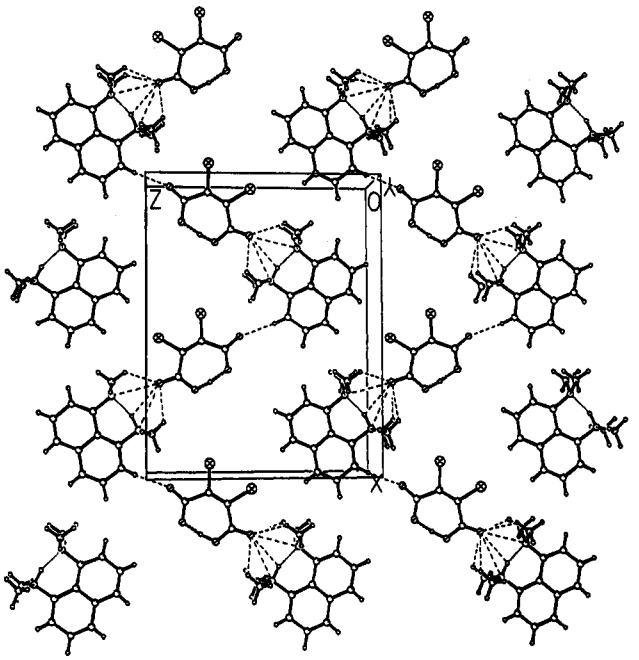

Figure 3. Characteristic zig−zag arrangement of the molecular plane in DMANH$^+$ClMH$^-$.

C5C6, O1aC1a, and O2aC1a bond lengths, and 1.0(3)° and 0.8(3)° for C14N2C14a and C4C10C5 bond angles, respectively. The differential electron density map at 120 K obtained with the proton removed from the [N−H···N]$^+$ hydrogen bridge reveals two maxima. The higher is near the N2 atom and the lower near the N1 atom (Figure 4). This would suggest a possible disorder of the position of hydrogen in the [N−H···N]$^+$ hydrogen bond, but attempts to refine the two hydrogens with partial occupation factors failed.

As other hydrogen maleates, the hydrogen 1,2-dichloromaleate anion forms an anionic intramolecular [O−H···O]$^-$ hydrogen bond with O4a−H1oo = 1.24(5) Å, O2a···H1oo = 1.34(5) Å, O2a···O4a = 2.376(4) Å, and O2aH1ooO4a = 172(4)°. These values are typical for a strong, potentially symmetric hydrogen bond. The difference between the O4a−H1oo and O2a···H1oo bond lengths is not significant if the level

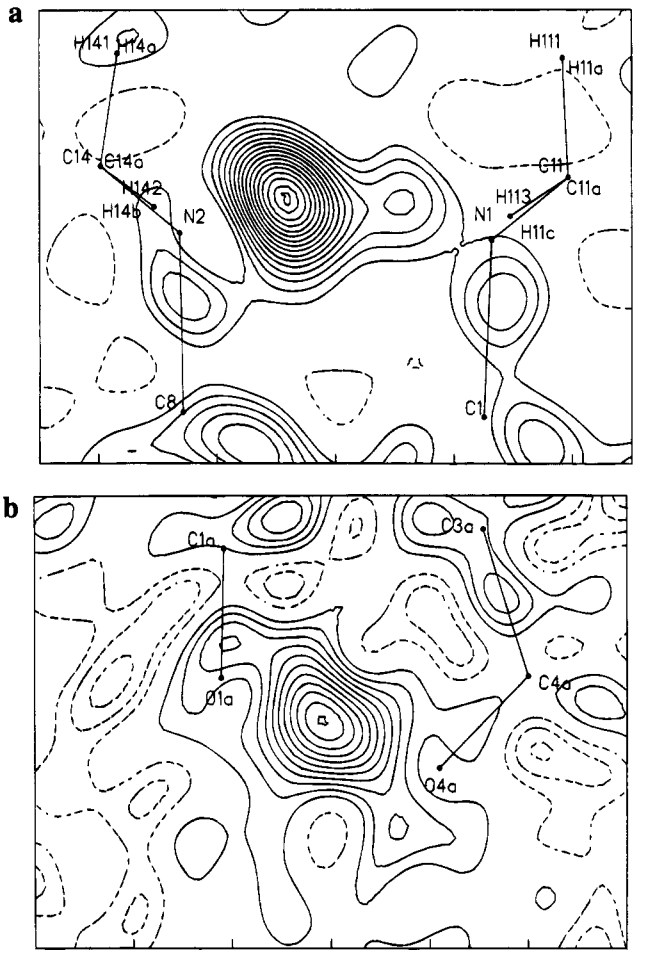

Figure 4. Differential electron density maps at 120 K obtained by removing a proton from the [N−H···N]$^+$ (a) and [O−H···O]$^-$ (b) hydrogen bonds. The contours are drawn in 0.05 e Å^{-3} intervals. The scale is in Å units.

of errors is taken into account. These conclusions are supported by the differential electron density map at 120 K (Figure 4) which reveals one broad maximum near the center of the O2a···O4a distance. Other differences between similar bond lengths and bond angles in the two halves of the anion are also

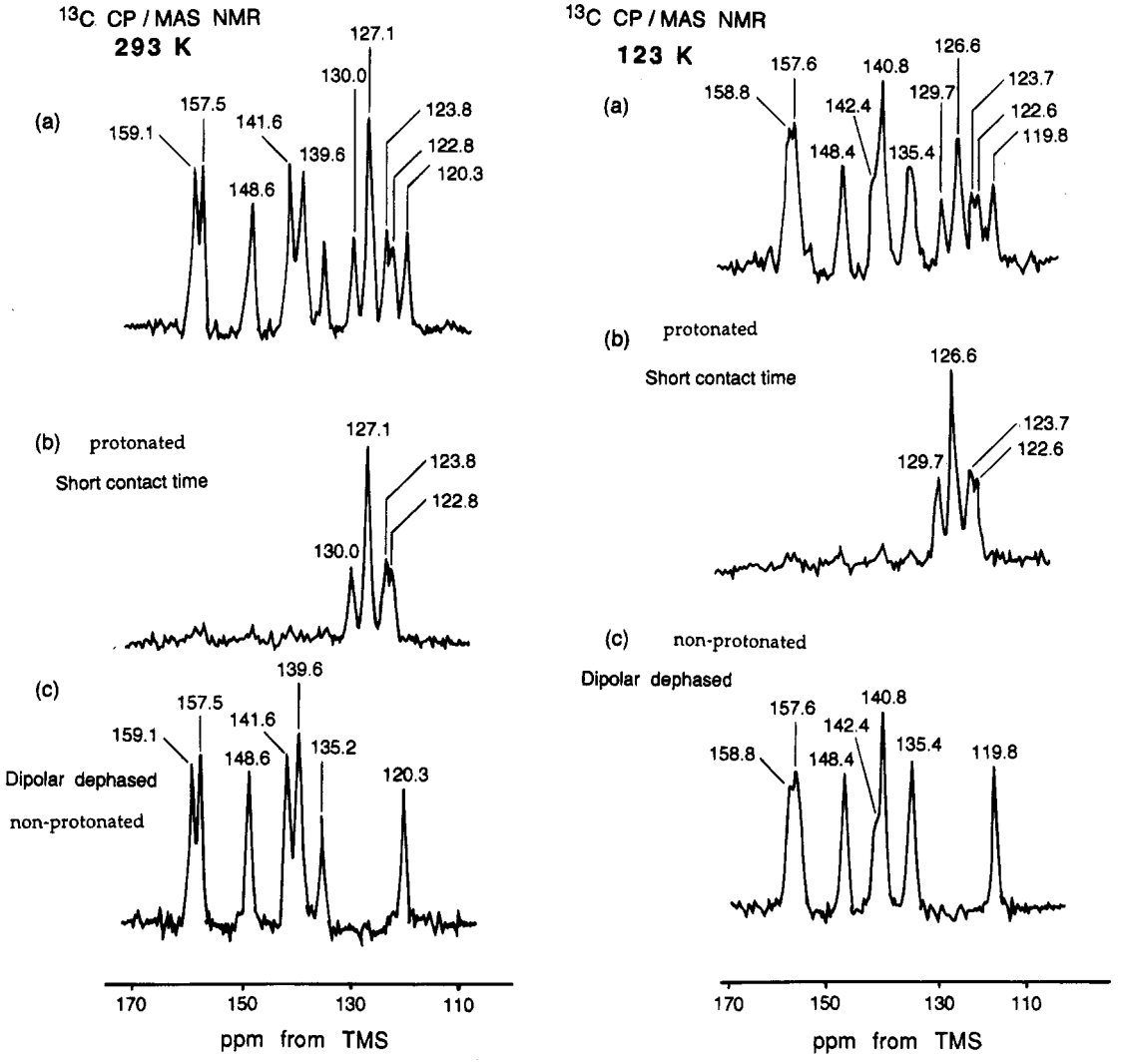

Figure 5. Aromatic regions of the $^{1}H-^{13}C$ CP/MAS NMR spectra of $DMANH^{+}ClMH^{-}$ at 293 K (left) and 123 K (right). (a) ^{13}C CP/MAS NMR spectrum, (b) short-contact-time spectrum, and (c) dipolar-dephased spectrum.

not significant. We believe that the donor–acceptor distance (O2a···O4a), which in most hydrogen maleate salts is larger than 2.4 Å,[36-44] is the shortest O···O distance ever found for the anion. The formation of the intramolecular $[O-H\cdots O]^{-}$ hydrogen bond is accompanied by the deformation of the C–C–C bond angles in the anion, 130.7(3)° and 129.8(3)° for C4aC3aC2a and C1aC2aC3a, respectively. The presence of two Cl atoms in positions 1 and 2 significantly increases the lengths of the C1aC2a, C2aC3a, and C3aC4a bonds, additionally increasing the electropositivity of carbons in both carboxylic groups compared with the nonsubstituted anion in a similar complex with DMAN.[15]

Solid-State NMR. At both temperatures the ^{1}H MAS NMR spectra of the complex (not shown) give broad peaks with maxima at 3.0 and 7.1 ppm (273 K) and 2.5 and 6.6 ppm (123 K) from hydrogens attached to aliphatic and aromatic carbons, respectively. The resonances from the protons involved in the $[N-H\cdots N]^{+}$ and $[O-H\cdots O]^{-}$ hydrogen bonds appear at 18.2 ppm (273 K) and 18.0 ppm (123 K). Both resonances are overlapped thus producing a more intense peak than in the case of other DMAN salts.[7,9] The differences in the chemical shifts at the two temperatures are not sufficiently significant to be interpreted.

The ^{13}C resonances have been assigned by reference to the literature.[7-9,14,15] At both temperatures, the aliphatic region of the $^{1}H-^{13}C$ CP/MAS NMR spectra (not shown) contains only one resonance from the methyl carbons. Given the location of the cation in the *m* symmetry plane, one would expect two signals. The chemical shift of the methyl carbon resonance is 46.1 ppm at 293 K and 45.4 ppm at 123 K, typical values intermediate between the chemical shifts of the in-plane and out-of-plane methyl groups in fully asymmetric cations.[9]

The $^{1}H-^{13}C$ CP/MAS NMR, short-contact-time and dipolar-dephased spectra of the aromatic region of $DMANH^{+}ClMH^{-}$ are shown in Figure 5. Unlike for the methyl group resonances, no spectral averaging is found. The top spectra contain peaks from all aromatic carbons in the complex, while the short-contact-time spectra only resonances from protonated carbons and the dipolar-dephased spectra contain only resonances from quaternary carbons. The higher resolution of the room temperature spectra is due to the more efficient averaging caused by the larger amplitude of the thermal motions of atoms. There are four lines in the short-contact-time spectra from the six carbons. This means that for the first time at least one pair of similar protonated carbon nuclei (C2 and C7, C3 and C6, C4 and C5) in the two halves of the cation gives separate resonances. Closer inspection of the short-contact-time spectra reveals that the highest peak (at ca. 127 ppm) must be the result of a superposition of three other peaks. Either each of these overlapping peaks comes from another pair of the similar nuclei or the total peak is the sum of two peaks from one pair of similar nuclei and one peak from another pair. The second possibility seems to be more likely. According to refs 7, 9, and 15, peaks from C3 and C6 carbons can be expected at ca. 127 ppm. Peaks from C2, C7 and C4, C5 are at ca. 123 and 130 ppm. Similarly, the resonances from the quaternary C1 and C8 carbons in the

TABLE 5: Peak Assignment in the ^1H and ^{13}C NMR Spectra of $DMANH^+ClMH^-$

atom	chemical shift (ppm) 293 K	123 K
C1, C8 (quaternary)	148.6	148.4
C2, C7 (protonated)	123.8,122.8	123.7, 122.6
C3, C6 (protonated)	127.1	126.6
C4, C5 (protonated)	130.0, 127.1	129.7, 126.6
C9 (quaternary)	120.3	119.8
C10 (quaternary)	135.2	135.4
C11, C12, C13, C14	46.1	45.4
H (Me)	3.0	2.5
H (aromatic)	7.1	5.6
H (acidic)	18.2	18.0
C1a, C4a	159.1, 157.5	158.8, 157.6
C2a, C3a	141.6, 139.6	142.4, 140.8

dipolar-dephased spectra are expected at ca. 148 ppm, from C9 at 120 ppm, and from C10 at ca. 135 ppm. This means that the remaining two split peaks (at ca. 158 and 140 ppm) must come from the quaternary carbons of the anion. Thus each carbon of the anion gives a separate peak. As a result of the less efficient averaging at 123 K, the separation between C1a and C4a and between C2a and C3a peaks is very small. The complete spectral assignment is given in Table 5.

ESCA. The variation of binding energies, quantified in terms of the ESCA chemical shift, is an important source of information on the chemical state of an atom. Despite many attempts to calculate chemical shifts and absolute binding energies, the factors involved, especially in the solid state, are so complex that any assignment must still rely on the literature data.

An ESCA spectrum is a plot of electron binding energy versus the number of electrons in a fixed narrow energy interval. There are several characteristic features of the C(1s) spectrum of $DMANH^+ClMH^-$ (Figure 6a). The large peak with maxima at 285.0 and 285.6 eV and shoulders at 284.6 eV (used as a binding energy reference), 286.1, and 287.0 eV may be associated with all the carbons except the two carboxylic carbons of the anion. Being partially positively charged, these two carbons have the largest binding energies of 289.2 and 288.4 eV. The presence of oxygen normally increases the C(1s) binding energies by 1.5 eV per C−O bond, which is why these two peaks are observed separately. The presence of asymmetric hydrogen bonds enables a partial assignment of the peaks. Because the proton is slightly closer to the donor O1a atom than to the acceptor O4a atom, the donor COOH group is less negatively charged than the acceptor COO− group. As a consequence, C1a is expected to have a higher 1s binding energy (289.2 eV) than the almost equivalent C4a atom (288.4 eV). The binding energies of these two carbons are additionally increased (by ca. 0.3 eV) by the secondary substituent effects of the Cl1 and Cl2 atoms.

The difference in binding energies of atoms in hydrogen donor and hydrogen acceptor groups can be used as a measure of the strength of hydrogen bonding. In the case of the $ClMH^-$ anion, the difference in the C(1s) binding energies is 0.8 eV. Ideally, one would like to use a reference system not involving hydrogen bonds. There may, however, be additional minor contributions to this difference from the mainly asymmetric intermolecular interactions of the oxygen atoms from the carboxylic groups with their nearest environment. An example of such interactions is the weak C−H···O hydrogen bonds: O2a($-X$, $-Y$, 2 − Z)···H142 = 2.49 Å and O1a(X, Y, 2 − Z)···H7 = 2.31 Å. The equivalent O3a and O4a atoms do not have such short intermolecular contacts. These short contacts may induce differences in the relative electronegativities of the oxygen atoms and should modify their primary and secondary substituent effects. However, because the C−H···O hydrogen bonds are far weaker than the anionic $[O-H\cdots O]^-$ hydrogen bond, their influence should be at least an order of magnitude smaller than in the case of the $[O-H\cdots O]^-$ bond. A similarly small difference in the secondary substituent effects of the Cl atoms can also be expected.

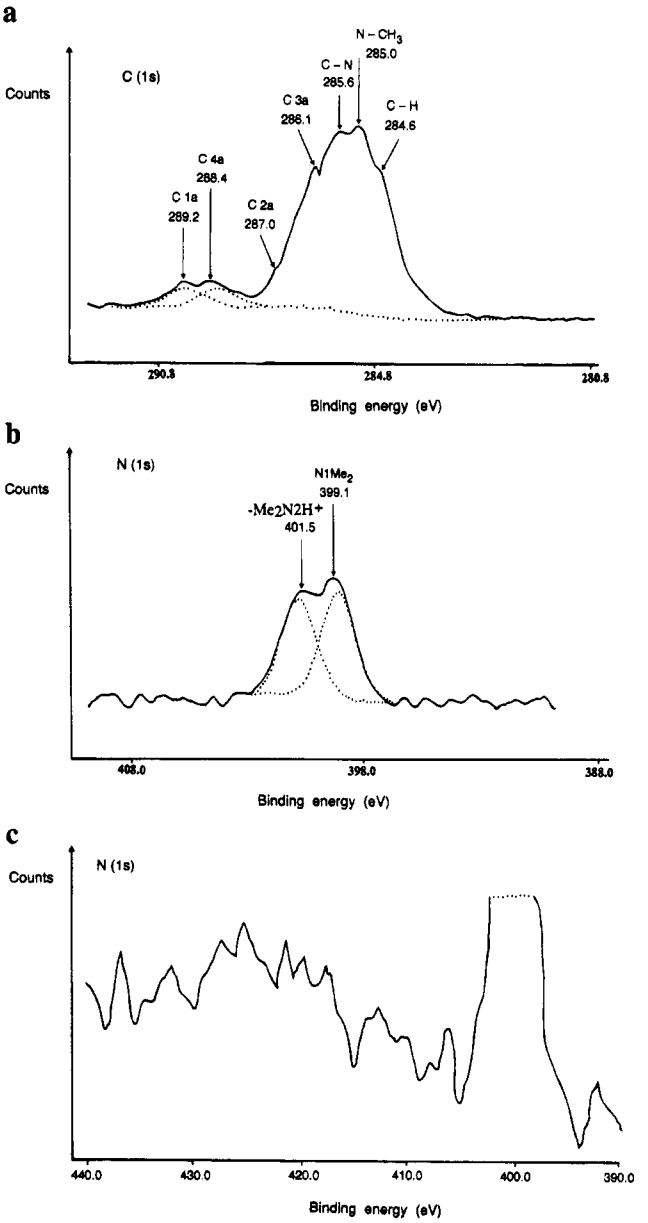

Figure 6. (a) C(1s) ESCA spectrum of $DMANH^+ClMH^-$, (b) N(1s) ESCA spectrum of $DMANH^+ClMH^-$, and (c) N(1s) ESCA loss spectrum of $DMANH^+ClMH^-$.

The shoulders at ca. 287.0 and 286.1 eV probably come from the C3a and C2a atoms. Their shift toward higher binding energies is caused by the primary and secondary substituent effects of chlorine (ca. 1.5 and 0.3 eV) and by the secondary substituent effects of the $[O-H\cdots O]^-$ hydrogen bond. The binding energy difference between these two lines is mainly the result of the differences between donor and acceptor oxygen atoms. The next two peaks at 285.6 and 285.0 eV are the result of a superposition of the broad $C-NR_1R_2$ and $N-CH_3$ carbon peaks with a peak from C−H carbons and a peak from the contaminant adventitious carbon, given that the sample was not prepared under a controlled atmosphere. The adventitious carbon peak normally comes from polymeric hydrocarbon species and reflects the presence of a variety of carbon−oxygen species.

The N(1s) spectrum of $DMANH^+ClMH^-$ (Figure 6b) contains two well-separated peaks with maxima at 401.5 and 399.1

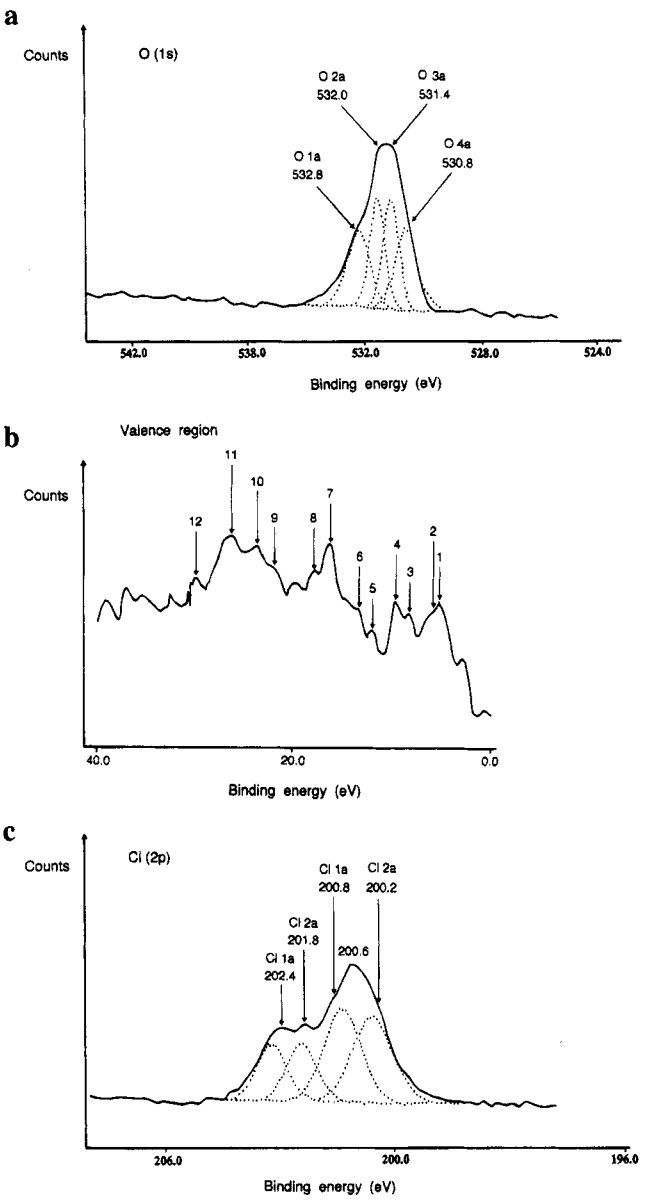

Figure 7. (a) O(1s) ESCA spectrum of $DMANH^+ClMH^-$, (b) valence band spectrum of $DMANH^+ClMH^-$, and (c) Cl(2p) ESCA spectrum of $DMANH^+ClMH^-$.

eV which can be uniquely assigned to the N2 and N1 nitrogen atoms, respectively. The attachment of the proton to the N2 nitrogen increases its binding energy compared with that of the acceptor N1 atom. The difference between the binding energies of these two atoms (1.8 eV) is yet another measure of the strength of the $[N-H\cdots N]^+$ hydrogen bond. However, also in this case the asymmetric intermolecular interactions with the nearest environment can, in a minor manner, contribute to this difference. In addition to the N(1s) features, the N(1s) loss spectrum of $DMANH^+ClMH^-$ exhibits characteristic features (Figure 6c). These include a hump in the ca. 415–430 eV range brought about by the loss of a specific amount of energy due to the interactions between the photoelectron and other electrons in the surface region of the sample. The energy interval between the primary peak and the loss peak is known as the plasmon energy (ca. 22.5 eV for $DMANH^+ClMH^-$).

The O(1s) spectrum of $DMANH^+ClMH^-$ contains a broad peak 3 eV wide (Figure 7a) with the maximum at ca. 531.1 eV and small shoulders at 532.3 and 530.0 eV. This may be deconvoluted into four peaks with maxima at 530.8, 531.4, 532.0, and 532.8 eV. The anion contains four different oxygens: O1a, O2a, O3a, and O4a. Since O1a and O4a participate in the asymmetric hydrogen bonding, the difference

TABLE 6: Core Electron Binding Energies in $DMANH^+ClMH^-$

region	peak assignment	binding energy [eV]	fwhm[a]
C(1s)		288.8	1.8
		285.3	2.4
	C1a	289.2	1.0
	C4a	288.4	1.0
	C2a	287.0	
	C3a	286.1	
	C–N	285.6	
	$N-CH_3$	285.0	
	C–H	284.6	
N(1s)		400.9	2.4
	N1	399.7	1.7
	N2	401.5	1.8
O(1s)		531.7	2.4
	O1a	532.8	1.0
	O2a	532.0	0.8
	O3a	531.4	0.8
	O4a	530.8	1.2
Cl(2p)		202.1	2.8
		200.5	3.0
	Cl1a	202.4	2.0
		200.8	2.0
	Cl2a	201.8	1.6
		200.2	2.0

[a] fwhm stands for full width at half-maximum.

between chemical shifts for these two oxygen atoms should be far greater than for the other pair. This suggests that the first and the fourth peaks in Figure 6a should be assigned to atoms O1a and O4a. O1a will have higher binding energy than O4a because it is less negatively charged due to its closer proximity to H1oo. The other pair of peaks can then be assigned to the O2a and O3a oxygens. Again, due to asymmetric $[O-H\cdots O]^-$ hydrogen bonding and the $O2a\cdots H-C$ hydrogen bond, O2a should have higher binding energy than O3a. The complete assignment of peaks is given in Table 6 and Figure 7a. The difference between the donor (O1a) and acceptor (O4a) oxygen core 1s binding energies is 2.0 eV and for the carbonyl oxygens O2a and O3a 0.6 eV. Also in this case the differences in the intermolecular interactions of the almost symmetric oxygens can slightly modify the differences in their binding energies.

Another independent confirmation of these conclusions is in the O(2s) fragment of the valence region (defined as the first ca. 20–30 eV of the binding energy) of the spectrum of $DMANH^+ClMH^-$ (Figure 7b). This contains mainly the energy levels which are involved in delocalized or bonding orbitals and has a "fingerprint" character. In the case of $DMANH^+ClMH^-$, the valence region consists of a superposition of a broad energy band from the delocalized π bonds of the complex with the better-defined peaks characteristic of the particular atoms. All valence peaks of the carbon, nitrogen, oxygen, and chlorine atoms can be expected in binding energy intervals characteristic for a given atom and a given energy level. For example, the $O(2p_{1/2})$, $Cl(3p_{1/2})$, and $N(2p_{1/2})$ peaks are expected in the energy range ca. 6–8 eV. $C(2p_{1/2})$ will then appear at ca. 11 eV and $H(1s_{1/2})$, $O(2p_{3/2})$, and $N(2p_{1/2})$ at ca. 12–15 eV. $Cl(3s_{1/2})$ and $C(2s_{1/2})$ are found at ca. 18 eV and $O(2s_{1/2})$ at ca. 24 eV. Again, the presence of hydrogen bonds and different substituent effects can modify the positions of these peaks. This is clearly observed for the $O(2s_{1/2})$ peaks and is very useful for the assignment of the peaks proposed in Table 7. These peaks can be assigned in a similar manner to the O(1s) peaks. Again, the largest positively shifted peak at ca. 31.8 eV comes from O1a and peaks at 27.6, 25.2, and 23.6 eV from the other oxygen atoms. The positions and shapes of these peaks are very informative when compared with the spectra of related compounds. Because the complex under study is an insulator, its valence band is separated from the empty conduc-

TABLE 7: ESCA Parameters for the Valence Region

peak no.	peak assignment	binding energy [eV]
1	$C(2p_{1/2})$	6.0
2	$O(2p_{1/2})$	8.8
3	$N(2p_{1/2})$	9.3
4	$C(2p_{1/2})$	10.6
5	$Cl(3p_{1/2})$	12.9
6	$H(1s_{1/2})O(2p_{3/2})$	14.4
7	$Cl(3s_{1/2})$	17.6
8	$C(2s_{1/2})$	18.9
	$O(2s_{1/2})$	ca. 24
9	O4a	23.6
10	O3a	25.2
11	O2a	27.6
12	O1a	31.4

tion band by a gap and the measured intensity of signals decreases to zero when the binding energy tends to zero.

The Cl(2p) spectrum (Figure 7c) contains further informative features. First, we note that the non-s-levels spectra give a doublet of peaks with the area ratio being a function of an electron subshell. The doublets arise through spin−orbit (j−j) coupling. When the orbital quantum number l is unity, two possible states must be considered for j ($j = 1 + s$) because the spin quantum number s can take two values ($\pm^1/_2$). The relative intensities of the members of the doublet are given by the ratio of their respective degeneracies ($2j + 1$; 1:2 for the p subshell). This is why two pairs of smaller and larger peaks are found in the Cl(2p) spectrum (Figure 7c). The entire spectrum can be deconvoluted into four peaks, two small and two large. The symmetry constraints were used to keep the ratio of the areas of the smaller peaks at unity (the same is true for the larger peaks) and the ratio of the areas of a smaller peak to a larger peak at 1:2. As a result, the peaks at 202.4 and 200.8 eV may be assigned to Cl1a and the 201.8 and 200.2 eV peaks to Cl2a. The difference in the binding energies of the smaller peak and the larger peak within each pair (1.6 eV) reflects the nature of the relation between the spin and orbital angular momenta of the remaining electron. The magnitude of this energy separation is proportional to the spin-orbital coupling constant which depends on the expectation value $\langle(1/r^3)\rangle$ for the particular orbital where r is its distance to the nucleus. The chlorine atoms in the anion are inequivalent as a result of the asymmetric hydrogen bond. The Cl1a atom should have a slightly higher binding energy because it is separated by fewer bonds from the proton in the $[O-H\cdots O]^+$ perturbing hydrogen bond. We assign the peaks at 202.4 and 200.8 eV to Cl1a and the other two peaks to Cl2a. Another minor contribution to the constant difference of 0.6 eV between the binding energies of the chlorine atoms may be due to the asymmetric intermolecular interactions of these two chlorines.

We conclude that ESCA reveals a rational picture of the perturbation of the binding energies of the core electron densities of atoms in the $ClMH^-$ anion (Figure 8). The perturbing asymmetric location of hydrogen in the hydrogen bridge affects the core binding energies of all atoms of the anion. This effect decreases with the increased distance from the hydrogen bond site.

Hydrogen Bonding in Hydrogen Maleates. The $ClMH^-$ anion is very similar to unsubstituted hydrogen maleate anions. There are 37 unique hydrogen maleate complexes in the CSD refined with $R < 0.075$. This sample is sufficiently large to allow us to generalize the properties of hydrogen bonding in the anion. The REFCODEs of structures retrieved from the CSD are given in the Supporting Information. It appears that the hydrogen bond in the anion is asymmetric (Figure 9). The bond is very strong with the average values of structural parameters defined in Figure 8 . The nonbonded distances from

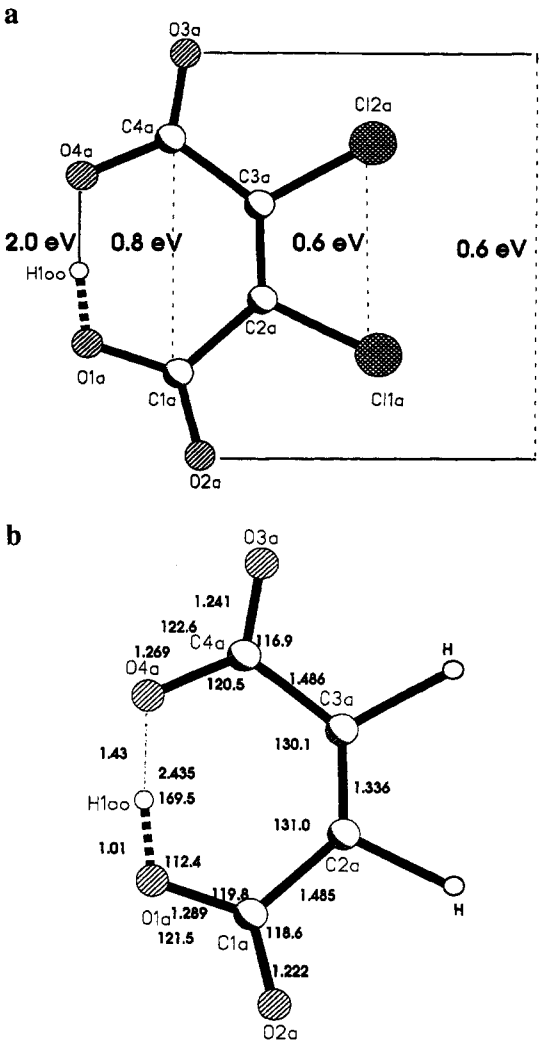

Figure 8. (a) Differences in binding energies of core electrons of symmetric atoms in the $ClMH^-$ anion and (b) average geometry of the $ClMH^-$ anion.

the hydrogen atom in the hydrogen bond to the third electronegative atom are never shorter than 3 Å, which demonstrates the strength of the shielding of the $-COO^-$ groups. The asymmetry of the $[O-H\cdots O]^-$ hydrogen bond is related to the asymmetry of intermolecular interactions of both carboxylic groups. Using the same labeling scheme as for $ClMH^-$, there are four slightly differently charged oxygens in the anion, O1a, O2a, O3a, and O4a, and the proton is nearer to O1a than O4a in the $[O1a-H1oo\cdots O4a]^-$ hydrogen bond. It appears that atoms O3a (Figure 9) and O2a, followed by O4a and O1a have the shortest nonbonded non-H-contacts. This is the reverse sequence in comparison with their geometric distance from H1oo in the hydrogen bond. It follows that even small differences in charges associated with similar atoms have an important influence on the three-dimensional arrangement of the molecules.

The relationship between hydrogen bonding and intermolecular interactions may also be inferred from the results of factor analysis. When all bonds (except C−H and O−H) of the anion are taken into account, the first factor obtained explains 60% of the total variation of the data. This factor may be written as a linear combination of the following bonds:

$$FACl = -C1aO2a + 1.5C1aO1a + 1.5C2aC3a - 1.5C4aO4a + 2C4aO3a$$

The contributions from C1aC2a and C3aC4a are not significant. Those from the proton-donor carboxylic group and the

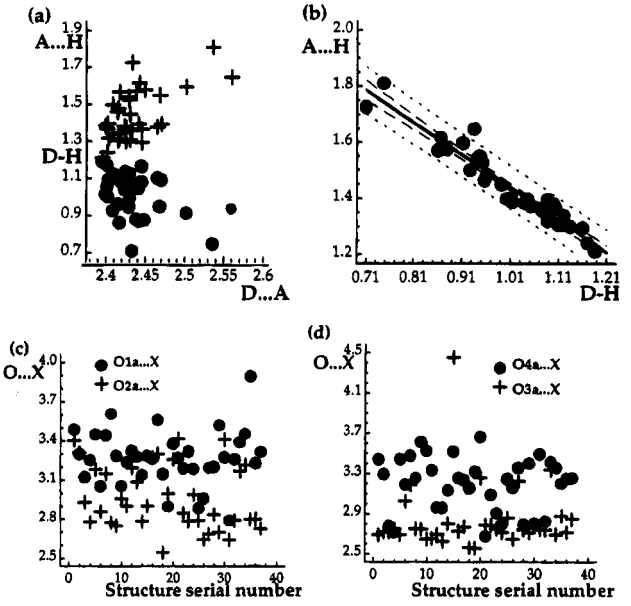

Figure 9. (a) Distribution of D−H and H···A distances vs donor−acceptor D···A distance in hydrogen maleates, (b) H···A distance vs D−H bond length (A···H = −1.15(5)D−H + 2.60(5), $R = -0.96$), (c) distribution of nonbonded distances of oxygen atoms in the proton donor carboxylic group, and (d) distribution of nonbonded distances of oxygen atoms in the proton-acceptor carboxylic group. All distances in Å.

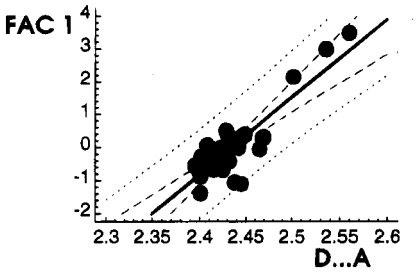

Figure 10. . Correlation between the first factor and the donor−acceptor O1a···O4a distance [Å] ($R = 0.87$).

protono-acceptor carboxylic groups have opposite signs, and the variation of C4aO3a is more significant than the variation of the C1aO2a bond nearer to the proton. The first factor correlates very well with the donor−acceptor O1a···O4a distance with a correlation coefficient $R = 0.87$ (Figure 10). The terminal oxygens not involved in hydrogen bonding are very sensitive to intermolecular interactions, and the resulting changes of their electronegativities are reflected in the properties of hydrogen bonding in hydrogen maleates.

Conclusions

Hydrogen bonding in the complex of 1,8-bis(dimethylamino)-naphthalene (DMAN) with 2,3-dichloromaleate has been investigated by using X-ray diffraction, ^{1}H and ^{13}C MAS NMR (both at room and low temperatures), and room temperature electron spectroscopy (ESCA). X-ray diffraction shows that the $[N-H\cdots N]^+$ hydrogen bond in $DMANH^+$ is asymmetric and the $[O-H\cdots O]^-$ hydrogen bond in the $ClMH^-$ anion is symmetric. The anion itself is also symmetric at the level of errors.

The asymmetry of hydrogen bonds is reflected in the values of chemical shifts in the ^{13}C NMR spectra. The geometric parameters of the complex are very similar at both temperatures and closely agree with the values obtained by ab-initio optimization. Protons located in both hydrogen bonds have large chemical shifts of ca. 19 ppm. We show the first ^{13}C CP/MAS NMR spectra of DMAN salts with partially resolved protonated carbon peaks.

It is clear that ESCA is a very useful tool for investigating hydrogen bonding at or near the surface of organic materials. The differences in the binding energies of the core (and valence) electrons of donor and acceptor atoms are a sensitive measure of the strength of hydrogen bonding. They may be used for the comparison of the strengths of different classes of hydrogen bonds with different heterodonors and acceptors when related to the binding energies of the same donor and acceptor atoms in reference compounds where these atoms do not participate in hydrogen bonding. In the case of $DMANH^+ClMH^-$ the $[O-H\cdots O]^-$ hydrogen bond is stronger than the $[N-H\cdots N]^+$ bond.

ESCA shows that the asymmetric hydrogen bonding in the $ClMH^-$ anion differentiates between the almost symmetrically located atoms of the moiety and its influence on the other atoms decreases with the increase of the geometric distance from the hydrogen bonding site. The asymmetry of the hydrogen bond in hydrogen maleates seems to result from asymmetric intermolecular interactions of carboxylic groups.

Acknowledgment. We are grateful for the Royal Society Research Fellowship for K.W and to the Department of Chemistry, University of Warsaw, for partial support from the project 12-501/VII/BW-1301/41/95.

Supporting Information Available: Tables of anisotropic displacement parameters for $DMANH^+ClMH^-$ at 120 and 293 K and table of REFCODEs and structural parameters of hydrogen maleates (4 pages); tables of observed and calculated structure factors for $DMANH^+ClMH^-$ at 120 and 293 K (10 pages). Ordering information is given on any current masthead page.

References and Notes

(1) *Practical Surface Analysis*, 2nd ed.; Briggs, D., Seah, M. P., Eds.; John Wiley: New York, 1980.
(2) Barr, T. L. *Modern ESCA;* CRC: Boca Raton, FL, 1994.
(3) Wagner, C. D.; Riggs, W. M.; Davis, L. E.; Moulder, J. F.; Muilenberg, G. E. *Handbook of X-Ray Photoelectron Spectroscopy;* Perkin-Elmer Corp.: Eden Prairie, MN 1979.
(4) Staab, H. A.; Saupe, T. *Angew. Chem., Int. Ed. Engl.* **1988**, *27*, 865.
(5) Alder, R. *Chem. Rev.* **1989**, *89*, 1215.
(6) Einspahr, H.; Robert, J.-B.; Marsh, R. E.; Roberts, J. *Acta Crystallogr.* **1973**, *B29*, 1611.
(7) Wozniak, K.; He, H.; Klinowski, J.; Nogaj, B.; Lemanski, D.; Hibbs, D.; Hursthouse, M. B.; Howard, S. T. *J. Chem. Soc., Faraday Trans.*, in press.
(8) Grech, E.; Stefaniak, L.; Ando, I.; Yoshimizu, H.; Webb, G.; Sobczyk, L. *Bull. Chem. Soc. Jpn.* **1990**, *63*, 2716. Grech, E.; Stefaniak, L.; Ando, I.; Yoshimizu, H.; Webb, G. *Bull. Chem. Soc. Jpn.* **1991**, *64*, 3761.
(9) Wozniak, K.; He, H.; Klinowski, J.; Grech, E. *J. Phys. Chem.* **1991**, *99*, 1403.
(10) Stephenson, D.; Smith, J. A. S. *Proc. R. Soc. London* **1988**, *A416*, 149.
(11) Nogaj, B.; Wozniak, K.; Lemanski, D.; Ostafin, M.; Grech, E. *Solid State NMR* **1995**, *4*, 187.
(12) Platts, J. A.; Howard, S. T.; Wozniak, K. *J. Org. Chem.* **1994**, *59*, 4647.
(13) Allen, F. H.; Davies, J. E.; Galloy, J. J.; Johnson, O.; Kennard, O.; Macrae, C. F.; Mitchell, E. M.; Mitchell, G. F.; Smith, J. M.; Watson, D. G. *J. Chem. Inf. Comput. Sci.* **1991**, *31*, 187.
(14) Bartoszak, E.; Dega-Szafran, Z.; Grunwald-Wyspianska, M.; Jaskólski, M.; Szafran, M. *J. Chem. Soc., Faraday Trans.* **1995**, *91*, 87.
(15) Bartoszak, E.; Dega-Szafran, Z.; Grunwald-Wyspianska, M.; Jaskólski, M.; Szafran, M. *J. Chem. Soc., Faraday Trans.* **1993**, *89*, 2085.
(16) George, P.; Bock, C.; Trachtman, M. *J. Phys. Chem.* **1983**, *87*, 1839.
(17) Hodoscek, M.; Hadzi, D. *J. Mol. Struct. (THEOCHEM)*, **1990**, *209*, 411.
(18) *TeXsan, Single Crystal Structure Analysis Software*, Version 1.6; Molecular Structure Corporation: The Woodlands, TX 77381, 1993.

(19) Sheldrick, G. M. *Acta Crystallogr.* **1990**, *A46*, 467.
(20) Sheldrick, G. M. *J. Appl. Crystallogr.*, in press.
(21) *International Tables for Crystallography*; Wilson, A. J. C., Ed.; Kluwer: Dordrecht, 1992; Vol. C.
(22) Barr, T. L. *Rev. Anal. Chem.*, **1991**, *22*, 229.
(23) Barr, T. L. *Appl. Surf. Sci.* **1983**, *15*, 1.
(24) Truter, M. R.; Vickery, B. L. *J. Chem. Soc., Dalton Trans.* **1972**, 395.
(25) Pyzalska, D.; Pyzalski, R.; Borowiak, T. *J. Crystallogr. Spectrosc. Res.* **1983**, *13*, 211.
(26) Glowiak, T.; Malarski, Z.; Sobczyk, L.; Grech, E. *J. Mol. Struct.* **1987**, *157*, 329.
(27) Wozniak, K.; Krygowski, T. M.; Kariuki, B.; Jones, W.; Grech, E. *J. Mol. Struct.* **1990**, *240*, 111.
(28) Bartoszak, E.; Jaskólski, M.; Grech, E.; Gustafsson, T.; Olovsson, I. *Acta Crystallogr.* **1994**, *B50*, 358.
(29) Miller, P. K.; Abney, K. D.; Rappe, A. K.; Anderson, O. P.; Strauss, S. H. *Inorg. Chem.* **1988**, *27*, 2255.
(30) Brown, D. A.; Clegg, W.; Colquhoun, H. M.; Daniels, J. A.; Stephenson, J. R.; Wade, K. *J. Chem. Soc., Chem. Commun.* **1987**, 889.
(31) Kanters, J. A.; Schouten, A.; Kroon, J.; Grech, E. *Acta Crystallogr.* **1991**, *C47*, 807.
(32) Malarski, Z.; Lis, T.; Grech, E.; Nowicka-Scheibe, J.; Majewska, K. *J. Mol. Struct.* **1990**, *221*, 227.
(33) Kanters, J. A.; Ter Horst, E. H.; Kroon, J.; Grech, E. *Acta Crystallogr.* **1991**, *C47*, 224.
(34) Kellet, P. J.; Anderson, O. P.; Strauss, S. H.; Abney, K. D. *Can. J. Chem.* **1989**, *67*, 2023.
(35) Wozniak, K.; He, H.; Klinowski, J.; Jones, W.; Grech, E. *J. Phys. Chem.* **1994**, *98*, 13755.
(36) Gupta, M. P.; Yadav, B. *Cryst. Struct. Commun.* **1974**, *3*, 595.
(37) James, M. N. G.; Williams, G. J. B. *Acta Crystallogr. B* **1974**, *30*, 1249. Gupta, M. P.; Mahata, A. P. *Indian J. Phys.* **1975**, *49*, 74.
(38) Ellison, R. D.; Levy, H. A. *Acta Crystallogr.* **1965**, *19*, 260.
(39) Parvez, M. *Acta Crystallogr.* **1990**, *C46*, 943.
(40) Hsu, B.; Schlemper, E. O. *Acta Crystallogr.* **1980**, *B36*, 3017. James, M. N. G.; Matsushima, M. *Acta Crystallogr.* **1976**, *B32*, 1708.
(41) Drobez, S.; Golic, L.; Leban, I. *Acta Crystallogr.* **1985**, *C41*, 1503.
(42) Golic, L.; Leban, I.; Detoni, S.; Orel, B.; Hadzi, D. *J. Cryst. Spectrosc.* **1985**, *15*, 215.
(43) Gupta, M. P.; Van Alsenoy, C.; Lenstra, A. T. H. *Acta Crystallogr.* **1984**, *C40*, 1526.
(44) James, M. N. G.; Williams, G. J. B. *Can. J. Chem.* **1974**, *52*, 1872.

JP9516349